



τ_{B_s}/τ_{B_d} and $\Delta\Gamma_s$ confront new physics in $b \rightarrow s\tau\tau$

Marzia Bordone^{1,a} , Mario Fernández Navarro^{2,b}

¹ Theoretical Physics Department, CERN, 1211 Geneva 23, Switzerland

² School of Physics and Astronomy, University of Southampton, Southampton SO17 1BJ, UK

Received: 18 July 2023 / Accepted: 5 September 2023 / Published online: 22 September 2023
© The Author(s) 2023

Abstract Several new physics scenarios that address anomalies in B -physics predict an enhancement of $b \rightarrow s\tau\tau$ with respect to its Standard Model prediction. Such scenarios necessarily imply modifications of the lifetime ratio τ_{B_s}/τ_{B_d} and the lifetime difference $\Delta\Gamma_s$. In this work, we explore indirect bounds provided by these observables over new physics scenarios. We also estimate future projections, showing that future experimental and theoretical improvements on both τ_{B_s}/τ_{B_d} and $\Delta\Gamma_s$ have the potential to provide bounds competitive with those directly extracted from $b \rightarrow s\tau\tau$ transitions. After performing a model-independent analysis, we apply our results to the particular case of leptoquark mediators proposed to address the $R_{D^{(*)}}$ anomalies.

1 Introduction

The characterisation of new physics scenarios affecting flavour-changing processes is a challenging task. In fact, high theoretical and experimental accuracy is needed to extract significant constraints. Furthermore, a large set of observables is required to extract the complete flavour structure of the new physics couplings, and the compatibility between several constraints needs to be addressed. Interestingly, in recent years hints of lepton flavour universality violation in $b \rightarrow c\tau\bar{\nu}$ mediated processes have raised a lot of attention. In fact, the lepton flavour universality ratios $R_{H_c} = \mathcal{B}(H_b \rightarrow H_c\tau\bar{\nu})/\mathcal{B}(H_b \rightarrow H_c\mu\bar{\nu})$, with $H_{b(c)}$ hadrons with a $b(c)$ quark, show deviations with respect to their respective Standard Model predictions. In particular, the two ratios R_D and R_{D^*} drive the discrepancy, at the level of 3.2 standard deviations [1]. It is important to notice that, due to these deviations, a lot of progress has been achieved concerning Standard Model predictions, culminating with the impressive

results from Lattice QCD in predicting $B \rightarrow D^*$ hadronic form factors [2–4]. Despite the recent progress, these results show tensions among each other and with experimental data and hence require further investigation. For this work, we use the averaged predictions in [1]. Other observables beyond $R_{D^{(*)}}$ have been measured, namely $R_{J/\psi}$ [5] and R_{Λ_b} [6], which, however, are affected by large experimental errors. They are consistent with the current deviations in $R_{D^{(*)}}$, but they are not yet precise enough to shed light on this interesting puzzle.

In light of this, many Beyond the Standard Model scenarios have been hypothesized, with the introduction of new heavy states. Most of these scenarios, in order to accommodate the size of the discrepancy in $b \rightarrow c\tau\bar{\nu}$ decays, predict sizeable effects in $b \rightarrow s\tau\tau$ transitions, hence yielding a strong correlation between these two partonic processes. One of the most favourable ways of testing this correlation is using the bounds on $\mathcal{B}(B_s \rightarrow \tau\tau)$. However, with the increasing theoretical and experimental precision, it is natural to wonder whether it could be tested elsewhere. One of the possibilities is then looking at the lifetime difference of the B_s system, or the lifetime ratio with respect to the B_d meson. Both these observables are indeed modified by new physics in $b \rightarrow s\tau\tau$, and it can be studied if their foreseen precision allows extracting more information than with data on $\mathcal{B}(B_s \rightarrow \tau\tau)$. This is exactly the scope of this work. In Sect. 2 we briefly revise the theoretical framework and current status of the observables of interest. In Sect. 3, we perform a model-independent analysis, highlighting correlations between the different observables contributing. In Sect. 4, we work out the results for some explicit models. In Sect. 5, we conclude.

2 Setup and observables

The starting point of our analysis is to introduce New Physics (NP) in $b \rightarrow c\tau\bar{\nu}$ transitions. At the high scale $\mu = \Lambda$,

^a e-mail: marzia.bordone@cern.ch (corresponding author)

^b e-mail: M.F.Navarro@soton.ac.uk

where $SU(2)_L \times U(1)_Y$ invariance is restored, we have the following effective Lagrangian:

$$\mathcal{L}^{\text{eff}} = \mathcal{L}_{\text{SM}} - \frac{1}{\Lambda^2} \sum_i \tilde{C}_i(\mu) \mathcal{Q}_i, \tag{2.1}$$

where the relevant operators, defined according to the SMEFT basis in [7], are listed in Appendix A. At the low scale $\mu = m_b$, $SU(2)_L \times U(1)_Y$ gauge invariance is broken and the effective Lagrangian reads:

$$\mathcal{L}_{\text{eff}} = -\frac{4G_F}{\sqrt{2}} \sum_i C_i(\mu) \mathcal{O}_i \tag{2.2}$$

where the operators \mathcal{O}_i are in the LEFT basis [8]. At the tree-level, only semileptonic operators are generated, and they are listed in Eqs. (A.4)–(A.11). The tree-level matching between the Wilson coefficients of the aforementioned operators and the ones in the SMEFT is given in Appendix A, and the running between the scale $\mu = \Lambda \sim 1 \text{ TeV}$ and $\mu = m_b$ is evaluated using DsixTools 2.1 [9]. Non-zero contributions to four-quarks operators are induced at the loop level from semileptonic operators. The complete set of them is in Eqs. (A.12)–(A.14).

In the next subsection, we revise the mixing formalism of the B_s meson system in presence of NP operators induced by the semileptonic ones, and discuss current status and prospects.

2.1 $\Delta\Gamma_s$ and τ_{B_s}/τ_{B_d} beyond the Standard Model

The absorptive off-diagonal element of the time evolution of the neutral B_s meson system, Γ_{12}^s , and the dispersive one M_{12}^s , are closely related in the Standard Model. They define lifetimes, mass differences and CP asymmetry as, respectively,

$$\Delta\Gamma_s = 2|\Gamma_{12}^s| \cos \phi_s, \quad \Delta M_s = |M_{12}^s|, \\ a_{sl}^s = \text{Im} \left(\frac{\Gamma_{12}^s}{M_{12}^s} \right), \tag{2.3}$$

with the mixing phase $\phi_s = \arg(-M_{12}^s/\Gamma_{12}^s)$. Corrections to these equations amount to $\mathcal{O}(1/8 |\Gamma_{12}^s/M_{12}^s|^2 \sin^2 \phi_s) \sim \mathcal{O}(10^{-11})$ in the SM, and are negligible with the current level of precision.

In case of NP couplings, the possible contributions to ΔM_s and a_{sl}^s are closely linked to the UV completion of the various models. Hence, we postpone the discussion to the specific models in Sect. 4. Instead, for Γ_{12}^s , the NP contributions are always finite, and are related to the discontinuity of the diagram in Fig. 1. We follow the approach in Ref. [10], where NP $(\bar{s}b)(\bar{\tau}\tau)$ effective operators are inserted. For each possible NP operator, we obtain:

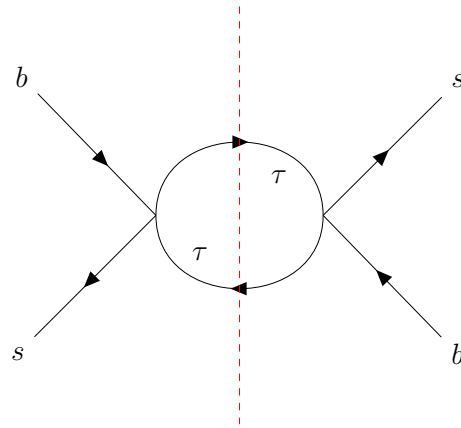


Fig. 1 Diagram that contributes to Γ_{12}^s via a double insertion of $(\bar{s}b)(\bar{\tau}\tau)$ operators. The tau loop in the diagram is closed and the cut (red dashed line) indicates that only the imaginary part of the graph is taken

$$(\Gamma_{12}^s)_{S,AB} = 3\mathcal{N}_{\Gamma_{12}^s} x_\tau \beta_\tau \left\langle Q_S^B \right\rangle \left([C_{ed}^{S,AB}]^{3323} \right)^2, \tag{2.4}$$

$$(\Gamma_{12}^s)_{V,LA} = \mathcal{N}_{\Gamma_{12}^s} \beta_\tau \left[(1 - x_\tau) \left\langle Q_V^L \right\rangle + (1 + 2x_\tau) \left\langle Q_S^R \right\rangle \right] \\ \times \left([C_{ed}^{V,LA}]^{3323} \right)^2, \tag{2.5}$$

$$(\Gamma_{12}^s)_{T,AA} = -12\mathcal{N}_{\Gamma_{12}^s} x_\tau \beta_\tau \left[4 \left\langle Q_S^A \right\rangle + 8 \left\langle \tilde{Q}_S^A \right\rangle \right] \\ \times \left([C_{ed}^{T,AA}]^{3323} \right)^2. \tag{2.6}$$

where $A = L, R, B = L, R$ and we have introduced $\beta_\tau = \sqrt{1 - 4x_\tau}$, $x_\tau = m_\tau^2/m_b^2$ and $\mathcal{N}_{\Gamma_{12}^s} = -G_F^2 m_b^2 / (6\pi M_{B_s})$. The corresponding expression for $(\Gamma_{12}^s)_{V,RA}$ can be obtained by exchanging the labels L and R everywhere. Note that each NP contribution is obtained by insertion of twice the same operator, since the interference between different operators is zero. Therefore, in the presence of more than one operator, the total NP contribution to Γ_{12}^s can be obtained by summing the contribution of each individual operator. While reviewing the calculation, we found a sign difference with respect to Eq.(E.3) in Ref. [10]. However, despite of this discrepancy, the final result in Eqs. (2.4)–(2.6) agrees with Eq. (60) in Ref. [10]. We define the matrix elements of the possible NP operators in the B_s field as

$$\left\langle Q_V^A \right\rangle = \langle \bar{B}_s | (\bar{s} \gamma_\mu P_A b) (\bar{s} \gamma^\mu P_A b) | B_s \rangle = \frac{2}{3} f_{B_s}^2 M_{B_s}^2 B_{B_s}^{(1)}, \\ \left\langle Q_S^A \right\rangle = \langle \bar{B}_s | (\bar{s} P_A b) (\bar{s} P_A b) | B_s \rangle \\ = -\frac{5}{12} \left(\frac{M_{B_s}}{m_b(\mu) + m_s(\mu)} \right)^2 f_{B_s}^2 M_{B_s}^2 B_{B_s}^{(2)}, \\ \left\langle \tilde{Q}_S^A \right\rangle = \langle \bar{B}_s | (\bar{s}_\alpha P_A b_\beta) (\bar{s}_\beta P_A b_\alpha) | B_s \rangle \\ = \frac{1}{12} \left(\frac{M_{B_s}}{m_b(\mu) + m_s(\mu)} \right)^2 f_{B_s}^2 M_{B_s}^2 B_{B_s}^{(3)}.$$

where α and β are color indices. The numerical input for the expressions above, including values for the bag parameters $B_{B_s}^{(i)}$, is given in Appendix B.

The ratio $\Delta\Gamma_s/\Delta\Gamma_s^{\text{SM}}$ is related to $\Gamma_{12}^{s,\text{NP}}$ through the following general expression:

$$\frac{\Delta\Gamma_s}{\Delta\Gamma_s^{\text{SM}}} = \left| 1 + \frac{\Gamma_{12}^{s,\text{NP}}}{\Gamma_{12}^{s,\text{SM}}} \frac{\cos\left[\phi_s^{\text{SM}} + \arg\left(1 + \frac{\Gamma_{12}^{s,\text{NP}}}{\Gamma_{12}^{s,\text{SM}}}\right)\right]}{\cos\phi_s^{\text{SM}}} \right|. \tag{2.7}$$

If we assume real NP Wilson coefficients, i.e. $\Gamma_{12}^{s,\text{NP}}$ is real, and neglect ϕ_s^{SM} along with the small phase of $\Gamma_{12}^{s,\text{SM}}$, then we arrive to the common formula found in the literature [10, 11]

$$\frac{\Delta\Gamma_s}{\Delta\Gamma_s^{\text{SM}}} = 1 + \frac{\Gamma_{12}^{s,\text{NP}}}{|\Gamma_{12}^{s,\text{SM}}|}. \tag{2.8}$$

Using the current SM prediction for $\Delta\Gamma_s$ [12], and the HFLAV average [1] we obtain for the ratio of the decay width difference

$$\frac{\Delta\Gamma_s}{\Delta\Gamma_s^{\text{SM}}} = 1.11 \pm 0.26, \tag{2.9}$$

which defines the space allowed for new physics. Similarly, the future projection is given by [13]

$$\left(\frac{\Delta\Gamma_s}{\Delta\Gamma_s^{\text{SM}}}\right)_{2035} = 1.06 \pm 0.06. \tag{2.10}$$

With this input, we can extract model independent bounds on the size of NP contributions. By using the current data we find

$$\Gamma_{12}^{s,\text{NP}} < 0.022 \text{ ps}^{-1}, \quad (95\% \text{ CL}) \tag{2.11}$$

and considering the 2035 numerical projection for $\Delta\Gamma_s/\Delta\Gamma_s^{\text{SM}}$ included in Eq. (2.10), we obtain the projected bound

$$\left(\Gamma_{12}^{s,\text{NP}}\right)_{2035} < 0.0029 \text{ ps}^{-1}. \quad (95\% \text{ CL}) \tag{2.12}$$

The NP effects in $\bar{s}b\bar{\tau}\tau$ couplings affect also the lifetime ratio of B_s and B_d mesons. If we assume no NP effects in the B_d lifetime, we have:

$$\frac{\tau_{B_s}}{\tau_{B_d}} = \left(\frac{\tau_{B_s}}{\tau_{B_d}}\right)_{\text{SM}} \left(1 + \frac{\Gamma(B_s \rightarrow \tau\tau)_{\text{NP}}}{\Gamma(B_s)_{\text{SM}}}\right)^{-1}, \tag{2.13}$$

where we define $\Gamma(B_s \rightarrow \tau\tau)_{\text{NP}} = \Gamma(B_s \rightarrow \tau\tau)_{\text{total}} - \Gamma(B_s \rightarrow \tau\tau)_{\text{SM}}$, which encodes the NP contribution to the partial decay width. The expression for $\Gamma(B_s \rightarrow \tau\tau)_{\text{total}}$

can be extracted from Eq. (C.2). The SM prediction for the lifetime ratio can be found in Ref. [15], and it depends on non-perturbative parameters in the Heavy Quark Expansion as well as the size of $SU(3)_f$ breaking between the B_s and the B_d system. We employ the central values and errors for the expectation values of the next-to-leading power matrix element in the B_d field from [16]. Concerning the size of $SU(3)_f$ breaking, estimates using Heavy-Quark Effective Theory relations [15, 17] and preliminary Lattice QCD estimations [18, 19] are affected by large errors. To be very conservative, we use the central values from [17] and assign 100% errors. With this, we obtain:

$$\left(\frac{\tau_{B_s}}{\tau_{B_d}}\right)_{\text{SM}} = 1.02 \pm 0.02, \quad \Gamma(B_s)_{\text{SM}} = 0.597_{-0.069}^{+0.106} \text{ ps}^{-1}, \tag{2.14}$$

that is compared with the current experimental HFLAV average [1],

$$\left(\frac{\tau_{B_s}}{\tau_{B_d}}\right)_{\text{HFLAV2022}} = 1.001 \pm 0.004. \tag{2.15}$$

At the current status, we find good agreement between the SM predictions and the lifetime average, albeit with large uncertainties due to the unknown $SU(3)_f$ breaking.

We note that in the literature, it has been discussed the impact of using the values from a different set of non perturbative parameters in the lifetime ratio [15, 20], which yield to a large shift. However, it has to be noticed that the values for these parameters change a lot depending on whether higher dimensional operators are considered or not, hinting to non-trivial correlations. This is not observed in [16], that we adopt as our reference. We can now extract an indirect limit over NP contributions to $\mathcal{B}(B_s \rightarrow \tau\tau)$ from the lifetime ratio. Using Eq. (2.13), we obtain

$$\mathcal{B}(B_s \rightarrow \tau\tau)_{\text{NP}} < 5.5 \times 10^{-2}, \tag{2.16}$$

at the 95% CL, which has to be compared with the direct bound from LHCb [21], namely $\mathcal{B}(B_s \rightarrow \tau\tau)_{\text{NP}} < 6.8 \times 10^{-3}$. Currently, the direct bound over $\mathcal{B}(B_s \rightarrow \tau\tau)_{\text{NP}}$ obtained by the LHCb collaboration is 40% better than the indirect bound obtained from the lifetime ratio.

We then repeat this comparison with the projected sensitivities. The results are shown in Table 1. For the experimental measurement, we explore the possibility that the error will reduce to 1 per mille. For the SM prediction, we explore two hypotheses corresponding to either no change in the central value or a substantial reduction of it, towards a strong indication of small $SU(3)_f$ breaking. In hypothesis H1, we assume that the $SU(3)_f$ breaking parameters could be measured to a 10% precision, as possible in the foreseeable future using

Table 1 Projected bounds at 95% CL for $\mathcal{B}(B_s \rightarrow \tau\tau)_{\text{NP}}$ obtained from the lifetime ratio τ_{B_s}/τ_{B_d} are confronted against the projected bounds from LHCb [14]. For the projections in the lifetime ratio, we assume that the uncertainties will reduce to 1 per mille in the experiment. We display different results under two different hypothesis for the

SM prediction: that the central value will remain as the current one and the $SU(3)_F$ breaking parameters could be measured to a 10% precision (H1), and that the central value will shift to match the experiment and there is no $SU(3)_F$ breaking up to the per mille level (H2)

Assumptions	Input	$\mathcal{B}(B_s \rightarrow \tau\tau)_{\text{NP}}$		
		τ_{B_s}/τ_{B_d}	LHCb (50 fb ⁻¹)	LHCb (300 fb ⁻¹)
H1	$\left(\frac{\tau_{B_s}}{\tau_{B_d}}\right)_{\text{SM}} = 1.020(5)$	$1.7(6) \cdot 10^{-2}$		
	$\left(\frac{\tau_{B_s}}{\tau_{B_d}}\right)_{\text{exp}} = 1.001(1)$		$< 1.3 \cdot 10^{-3}$	$< 5 \cdot 10^{-4}$
H2	$\left(\frac{\tau_{B_s}}{\tau_{B_d}}\right)_{\text{SM}} = 1.001(1)$	$< 2.6 \cdot 10^{-3}$		
	$\left(\frac{\tau_{B_s}}{\tau_{B_d}}\right)_{\text{exp}} = 1.001(1)$			

Lattice QCD, but retaining the current central values, while in H2 we impose no $SU(3)_F$ breaking up to the per mille level. The LHCb collaboration provides two expected upper bounds for $\mathcal{B}(B_s \rightarrow \tau\tau)$: a first projection is based on a luminosity of 50fb⁻¹, which in contrast to the expectations in [14] will be reached only after 2032. The second upper bound from the LHCb collaboration is based on an expected luminosity of 300fb⁻¹, which with respect of the expectations in [14], will be reached only after 2041. This shows that improved measurements and predictions of the lifetime ratios have the potential of improving the current bound on $\mathcal{B}(B_s \rightarrow \tau\tau)$, while waiting for LHCb to collect the necessary statistics to obtain even more stringent bounds. This motivates extra efforts both from the theoretical and experimental communities to investigate τ_{B_s}/τ_{B_d} as a potential channel to constrain NP effects.

3 Model independent analysis

In this section, we employ the previous results to obtain bounds on the NP Wilson coefficients in a model independent way. We start by assuming that only the vector operators $[C_{ed}^{V,LL}]^{3323}$ and $[C_{de}^{V,LR}]^{3323}$ are non-zero. These operators are interesting because they contribute to both $C_9^{\tau\tau}$ and $C_{10}^{\tau\tau}$ via Eq. (C.9), which potentially receive bounds from our set of $b \rightarrow s\tau\tau$ observables. Moreover, we assume that $SU(2)_L$ invariance at high energies implies the connection,

$$[C_{ed}^{V,LL}]^{3323} \approx [C_{vedu}^{V,LL}]^{3332}, \quad (3.1)$$

which leads to correlations with $R_{D^{(*)}}$. The parameter space of $[C_{ed}^{V,LL}]^{3323}$ and $[C_{de}^{V,LR}]^{3323}$ is depicted in Fig. 2a. Currently, the most competitive bounds over the parameter space are given by the direct bounds on $\mathcal{B}(B_s \rightarrow \tau\tau)$ and $\mathcal{B}(B^+ \rightarrow K^+\tau\tau)$, followed by the indirect bounds obtained from the lifetime ratio τ_{B_s}/τ_{B_d} and from the lifetime difference $\Delta\Gamma_s$.

More interesting, however, is the future projected picture of the parameter space. Eventually, the strongest bounds are expected to come from updates by LHCb and Belle II, which will nevertheless require the collection of substantial integrated luminosity [14,22]. Following from our discussion of future projections in Sect. 2, it is not unreasonable that the lifetime ratio sets the strongest constraints over $C_{10}^{\tau\tau}$ -related scenarios for a certain period in the near future. Similarly, $\Delta\Gamma_s$ has the potential to set competitive constraints over scenarios involving both $C_9^{\tau\tau}$ and $C_{10}^{\tau\tau}$ until the next update of $\mathcal{B}(B^+ \rightarrow K^+\tau\tau)$ by Belle II.

In the particular NP scenarios where both primed and unprimed operators have similar size and sign, the NP contributions to $\mathcal{B}(B_s \rightarrow \tau\tau)$ and $\mathcal{B}(B^+ \rightarrow K^+\tau\tau)$ cancel, and the most competitive constraint becomes that of $\Delta\Gamma_s$. This is illustrated in Fig. 2c, where only $C_{10}^{\tau\tau}$ and $C_{10}'^{\tau\tau}$ are non-zero. We obtain that for $C_{10}'^{\tau\tau}/C_{10}^{\tau\tau} \approx 1.4$ the bound from $\Delta\Gamma_s$ is already the most competitive. This shows that potentially, better measurements of $\Delta\Gamma_s$ can help distinguish new physics scenarios characterised by similar NP couplings for left-handed and right-handed quarks, which naturally provide accidental cancellations in $\mathcal{B}(B_s \rightarrow \tau\tau)$.

In the following, we explore the parameter space of the scalar operators $[C_{ed}^{S,LL}]^{3323}$ and $[C_{ed}^{S,LR}]^{3323}$, which contribute to $C_S^{\tau\tau}$ and $C_P^{\tau\tau}$ via Eq. (C.10). We assume that $SU(2)_L$ invariance at high energies implies the connection,

$$[C_{ed}^{S,LR}]^{3323} \approx \left([C_{vedu}^{S,RL}]^{3332} \right)^*. \quad (3.2)$$

We illustrate the different bounds over the parameter space in Fig. 2b. Direct bounds over $\mathcal{B}(B_s \rightarrow \tau\tau)_{\text{NP}}$ and $\mathcal{B}(B^+ \rightarrow K^+\tau\tau)$ provide the strongest constraints over the parameter space when considering both current and projected bounds, but the lifetime ratio has the potential to provide very competitive bounds in the near future. Just like in the case of vector operators, in the particular NP scenarios where both primed

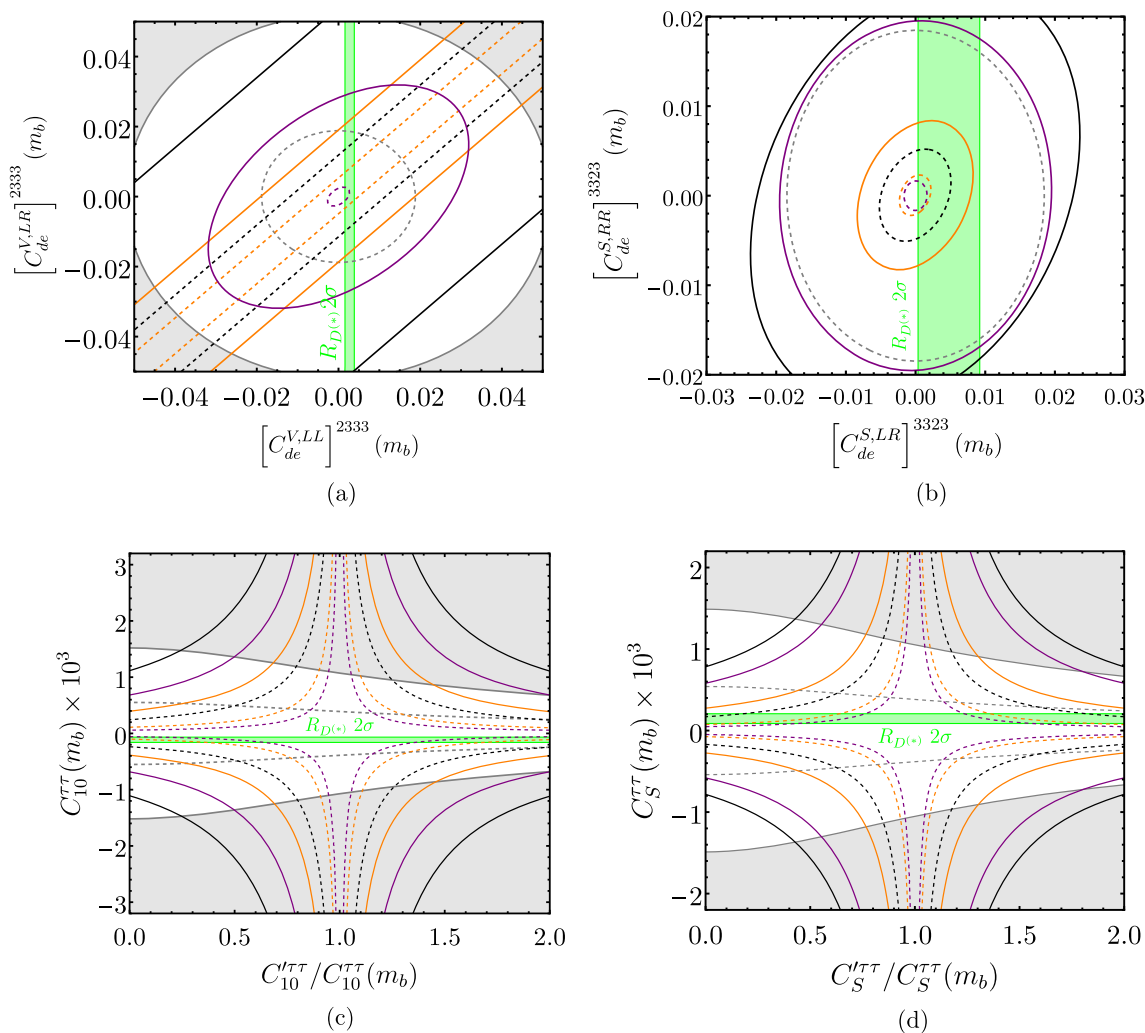


Fig. 2 (Top) Parameter space of vector (left) and scalar (right) Wilson coefficients (see the main text). (Bottom) Absolute size of $C_{10}^{\tau\tau}(m_b)$ vs the ratio $C_{10}^{\prime\tau\tau}(m_b)/C_{10}^{\tau\tau}(m_b)$ (left) and $C_S^{\tau\tau}(m_b)$ vs the ratio $C_S^{\prime\tau\tau}(m_b)/C_S^{\tau\tau}(m_b)$ (right). The plots in the bottom allow to study the parameter space in the scenario where both $C_{10(S)}^{\tau\tau}$ and $C_{10(S)}^{\prime\tau\tau}$ have similar size and sign. In all panels, orange contours represent the direct bounds over $\mathcal{B}(B_s \rightarrow \tau\tau)$, while the black contour represent the indirect

bounds over $\mathcal{B}(B_s \rightarrow \tau\tau)$ obtained from τ_{B_s}/τ_{B_d} , the purple contours represent the direct bounds over $\mathcal{B}(B^+ \rightarrow K^+\tau\tau)$, the grey contours represent the direct bounds over $\Delta\Gamma_s/\Delta\Gamma_s^{\text{SM}}$, and the green region is preferred by $R_{D^{(*)}}$ at 2σ . Solid (dashed) contours denote current (projected) 95% CL exclusions. For $\mathcal{B}(B_s \rightarrow \tau\tau)$, we show the projected direct bound by LHCb with 300 fb^{-1}

and unprimed scalar operators have similar size and sign, the NP contributions to $\mathcal{B}(B_s \rightarrow \tau\tau)$ and $\mathcal{B}(B^+ \rightarrow K^+\tau\tau)$ cancel, and the most competitive constraint becomes that of $\Delta\Gamma_s$. In this way, in Fig. 2d we explore the scenario where only $C_S^{\tau\tau}$ and $C_S^{\prime\tau\tau}$ are non-zero. We obtain that for $C_S^{\prime\tau\tau}/C_S^{\tau\tau} \approx 1.2$ the bound from $\Delta\Gamma_s$ is already the most competitive.

Finally, we note that, as already stated in Ref. [23], additional constraints will arise from future measurements of $B \rightarrow K^*\tau^+\tau^-$ and $B_s \rightarrow \phi\tau^+\tau^-$. In fact, being these decays a pseudovector to vector transition, they probe different combinations of Wilson coefficients, and provide stricter bounds on $C_9^{\tau\tau}$, hypothesising that the same potential sensitivity as for $B^+ \rightarrow K^+\tau^+\tau^-$ will be reached. Future projec-

tions taking into account the upcoming and current upgrade of the LHCb and Belle II experiments, can shed light on the actual constraining power of these modes.

4 New physics models

There is a rich literature about new mediators beyond the SM that have been proposed to explain the $R_{D^{(*)}}$ anomalies (see e.g. [24, 25]). In particular, leptoquarks constitute some of the most promising NP candidates, as they can naturally provide the required semileptonic operators while avoiding tree-level contributions to ΔM_s . Nevertheless, some of them predict an

enhancement of $b \rightarrow s\tau\tau$ observables much above their SM prediction, therefore potentially undergoing the constraints from τ_{B_s}/τ_{B_d} and $\Delta\Gamma_s$ derived in the previous sections. Furthermore, it has been shown that particular leptoquarks can also provide a one-loop and lepton universal contribution to the operator C_9 , which has been shown to greatly improve the global fit to $b \rightarrow s\ell\ell$ observables provided that the NP effect is roughly one fourth of the SM C_9 [26,27]. We denote such universal contribution as C_9^U , which specific leptoquarks can provide via RGE mixing from $C_9^{\tau\tau}$ and $C_{10}^{\tau\tau}$ [23,28].

We start by discussing scalar leptoquarks. Our conclusions can be summarised as in the following:

- The $S_1 \sim (\bar{\mathbf{3}}, \mathbf{1}, 1/3)$ leptoquark generates tree-level contributions to $R_{D^{(*)}}$, while $b \rightarrow s\tau\tau$ is only induced at loop level. Therefore, the correlation between these two modes is less strong and we checked explicitly that the loop induced effects in $b \rightarrow s\tau\tau$ are negligible for all the projected bounds considered in this paper.
- The $S_3 \sim (\bar{\mathbf{3}}, \mathbf{3}, 1/3)$ leptoquark induces both $R_{D^{(*)}}$ and $b \rightarrow s\tau\tau$ at the tree-level. However, leading constraints from $B \rightarrow K^{(*)}\nu\nu$ and ΔM_s render impossible to fully address the anomaly in $R_{D^{(*)}}$.
- The leptoquark $R_2 \sim (\mathbf{3}, \mathbf{2}, 7/6)$ provides uncorrelated contributions to $R_{D^{(*)}}$ and $b \rightarrow s\tau\tau$. The latter generates $C_9^U < 0$ via RGE mixing, therefore receiving constraints from τ_{B_s}/τ_{B_d} and $\Delta\Gamma_s$. However, we find that the leading constraint to this scenario comes from ΔM_s at 1-loop, that requires $|C_9^U| < 0.3$ in agreement with previous analyses [29]. Although a particular cancellation mechanism could alleviate the constraint from ΔM_s , this would require further model building beyond the scope of this work. Ultimately, even if ΔM_s is alleviated, the projected constraint from τ_{B_s}/τ_{B_d} could only rule out $|C_9^U| > 2$, unable to reach the region $C_9^U \approx -1$ preferred by global fits [26].

Vector leptoquarks are instead more promising. In the next subsections, we will study the ones that address $R_{D^{(*)}}$ while providing chirally enhanced contributions to $\mathcal{B}(B_s \rightarrow \tau\tau)$.

4.1 The vector leptoquark $U_1 \sim (\mathbf{3}, \mathbf{1}, 2/3)$

The $U_1 \sim (\mathbf{3}, \mathbf{1}, 2/3)$ vector leptoquark is a well motivated mediator to explain the R_D and R_{D^*} anomalies [30–37]. A well motivated embedding for gauge U_1 leptoquarks is the Pati-Salam group [38], that provides a natural connection with quark-lepton unification. Moreover, explanations of the $R_{D^{(*)}}$ anomalies via exchange of the U_1 vector leptoquark had been shown to be naturally connected with the origin of flavour hierarchies and the flavour structure of the SM [39–45]. Remarkably, the contributions of the U_1 vector leptoquark to $R_{D^{(*)}}$ are correlated to an enhancement of

$b \rightarrow s\tau\tau$. At an effective scale Λ higher than the electroweak scale, the U_1 interactions are well described in the context of the SMEFT as:

$$\mathcal{L}_{\text{SMEFT}}^{U_1} \supset -\frac{1}{\Lambda^2} \left[\frac{C_{LL}^{ij\alpha\beta}}{2} \left(Q_{\ell q}^{(1)} + Q_{\ell q}^{(3)} \right)^{ij\alpha\beta} - \left(2C_{LR}^{ij\alpha\beta} \left(Q_{\ell edq}^\dagger \right)^{ij\alpha\beta} + \text{h.c.} \right) \right]. \tag{4.1}$$

The matching between the relevant LEFT and SMEFT Wilson coefficients reads:

$$\left[C_{vedu}^{V,LL} \right]^{3332*}(m_b) = \eta_V^{\tau\nu} C_{LL}^{23\tau\tau}(\Lambda) \frac{v^2}{2V_{cb}\Lambda^2}$$

$$\left[C_{vedu}^{S,RL} \right]^{3332*}(m_b) = -\eta_S^{\tau\nu} 2C_{LR}^{23\tau\tau}(\Lambda) \frac{v^2}{2V_{cb}\Lambda^2}, \tag{4.2}$$

$$\left[C_{ed}^{V,LL} \right]^{3323}(m_b) = \eta_V^{\tau\tau} C_{LL}^{23\tau\tau}(\Lambda) \frac{v^2}{2\Lambda^2},$$

$$\left[C_{ed}^{S,LR} \right]^{3323}(m_b) = -\eta_S^{\tau\tau} 2C_{LR}^{23\tau\tau}(\Lambda) \frac{v^2}{2\Lambda^2}, \tag{4.3}$$

where the factors $\eta_i^{\tau\tau}$ and $\eta_i^{\tau\nu}$ encode the running from the high scale $\Lambda = 1 \text{ TeV}$ and are evaluated with DsixTools [46], obtaining $\eta_V^{\tau\tau} \simeq 0.96$, $\eta_S^{\tau\tau} \simeq 1.57$, $\eta_V^{\tau\nu} \simeq 1.03$ and $\eta_S^{\tau\nu} \simeq 1.64$. The operators in Eq. (4.3) match into $C_9^{\tau\tau} = -C_{10}^{\tau\tau}$ and $C_S^{\tau\tau} = -C_P^{\tau\tau}$ via Eqs. (C.9) and (C.10), respectively. The presence of the scalar operator $\left[C_{ed}^{S,LR} \right]^{3323}$, which ultimately provides $C_S^{\tau\tau} = -C_P^{\tau\tau}$, delivers a chirally enhanced contribution to $\mathcal{B}(B_s \rightarrow \tau\tau)$ connected to the size of $C_{LR}^{23\tau\tau}$. If $C_{LR}^{23\tau\tau} = 0$, then $\mathcal{B}(B_s \rightarrow \tau\tau)$ is still substantially enhanced by the presence of $C_9^{\tau\tau} = -C_{10}^{\tau\tau}$, but chiral enhancement is lost.

In Fig. 3 we explore the parameter space of SMEFT Wilson coefficients in the model, highlighting two particularly motivated benchmark scenarios. The case $C_{LL}^{23\tau\tau} = -C_{LR}^{23\tau\tau}$ is a good benchmark for 4321 models featuring TeV scale third family quark-lepton unification [30–32,39,42,43], while the case $C_{LR}^{23\tau\tau} = 0$ is a good benchmark for the flavour universal 4321 model [35,36,44,45]. Given that U_1 is a vector leptoquark, the leading contribution to ΔM_s arising at 1-loop depends on the specific UV completion. For the well-motivated case of 4321 models, the contribution to ΔM_s is dominated by a vector-like lepton running in the loop, and the most stringent constraints can be avoided as long as the mass of the vector-like lepton is around or below the TeV scale [31,36,45,47]. In this manner, the model is able to address $R_{D^{(*)}}$ and the enhancement of $\mathcal{B}(B_s \rightarrow \tau\tau)$ becomes a key prediction of the model.

Due to chiral enhancement, $\mathcal{B}(B_s \rightarrow \tau\tau)$ is particularly sensitive to scenarios with large $|C_{LR}^{23\tau\tau}|$, but current direct bounds from LHCb cannot yet test the preferred region by the benchmark case $C_{LL}^{23\tau\tau} = -C_{LR}^{23\tau\tau}$. Remarkably, in the near

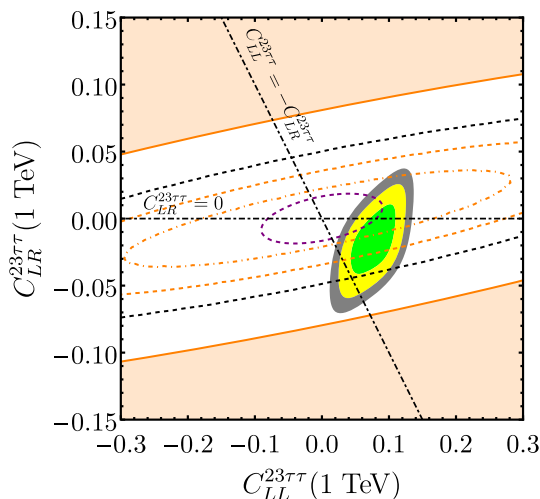


Fig. 3 Parameter space of Wilson coefficients motivated by the U_1 vector leptoquark explanation of $R_D^{(*)}$ (see main text). The green, yellow and grey regions represent the 1σ , 2σ and 3σ regions preferred by $R_D^{(*)}$, respectively. Orange contours represent the direct bounds from $\mathcal{B}(B_s \rightarrow \tau\tau)$, while the black contour represents the indirect bound obtained from τ_{B_s}/τ_{B_d} and the purple contour represents the direct bounds from $\mathcal{B}(B^+ \rightarrow K^+\tau\tau)$. Solid (dashed) contours denote current (projected) 95% CL exclusions, except for the two projections for $\mathcal{B}(B_s \rightarrow \tau\tau)$ by LHCb: 50 fb^{-1} (orange dashed) and 300 fb^{-1} (orange dash-dotted). Dash-dotted black lines represent two interesting benchmark scenarios motivated in the main text

future we expect the indirect bound from the lifetime ratio τ_{B_s}/τ_{B_d} to constrain a region of the parameter space preferred by $C_{LL}^{23\tau\tau} = -C_{LR}^{23\tau\tau}$, while the parameter space preferred by $C_{LR}^{23\tau\tau} = 0$ is expected to remain unconstrained. In the longer term, updated direct measurements of $\mathcal{B}(B_s \rightarrow \tau\tau)$ and $\mathcal{B}(B^+ \rightarrow K^+\tau\tau)$ have the potential to test most of the parameter space compatible with R_D and R_{D^*} .

As a final remark, using the results in [31, 36, 45, 47], and our aforementioned results for Γ_{12}^s , we estimated the NP impact on a_{sl}^s . However, due to absence of a NP phase in the relevant couplings, the NP contribution to a_{sl}^s is dominated by the phase of V_{ts}^* multiplied by small couplings. Hence, in this scenario we find no visible effect in a_{sl}^s . We notice that for complex right-handed couplings, this would not be the case, and would be worth studying it in detail if the misalignment between R_D and R_D^* changes significantly with new measurements.

4.2 The vector leptoquark $V_2 \sim (\bar{\mathbf{3}}, \mathbf{2}, 5/6)$

The vector leptoquark $V_2 \sim (\bar{\mathbf{3}}, \mathbf{2}, 5/6)$ arises in the context of grand unified theories (GUTs) based on the $SU(5)$ gauge group. In a recent work [48], it has been pointed out that a TeV scale V_2 vector leptoquark could explain the deviations in $R_{D^{(*)}}$ via the scalar operator $(\bar{c}_L b_R)(\bar{\tau}_R \nu_{L\tau})$, arising from the SMEFT operator $[Q_{ledq}^\dagger]^{\tau\tau 23}$. Notice that this operator is

also predicted by the U_1 vector leptoquark in models featuring third family quark-lepton unification at the TeV scale, and it has the interesting feature of correlating the enhancement of $R_{D^{(*)}}$ with a chiral enhancement of $\mathcal{B}(B_s \rightarrow \tau\tau)$. For the purpose of this work, we shall work with a simplified phenomenological Lagrangian, requiring only the minimal couplings needed to address the $R_{D^{(*)}}$ anomalies. In this manner, the di-quark coupling that would lead to a rapid proton decay is also absent. The relevant interaction terms read

$$\mathcal{L}_{V_2} \supset \beta_{i\alpha}^{dL} (\bar{d}^c_i \gamma_\mu L_\alpha^b) \epsilon_{ab} V_2^{\mu,a} + \beta_{i\alpha}^{Qe} (\bar{Q}^c_{i\alpha} \gamma_\mu e_\alpha) \times \epsilon_{ab} V_2^{\mu,b} + \text{h.c.} \tag{4.4}$$

where

$$\beta_{i\alpha}^{dL} = \begin{pmatrix} 0 & 0 & 0 \\ 0 & 0 & 0 \\ 0 & 0 & \beta_{3\tau}^{dL} \end{pmatrix}, \quad \beta_{i\alpha}^{Qe} = \begin{pmatrix} 0 & 0 & 0 \\ 0 & 0 & \beta_{2\tau}^{Qe} \\ 0 & 0 & 0 \end{pmatrix}. \tag{4.5}$$

As usual for leptoquarks, V_2 does not contribute to ΔM_s at tree level. Using DsixTools 2.1 [9], we have studied the 1-loop RGE mixing of $[Q_{ledq}^\dagger]^{\tau\tau 23}$ into low energy operators that could potentially contribute to ΔM_s and a_{sl}^s . We find all operators to receive vanishing contributions, with the exception of $[L_{dd}^{V,LL}]^{2323}$ that receives a negligible contribution at the level 0.0001% of the SM contribution. We stress that, in a UV complete model, we expect further states to be generated when breaking the $SU(5)$ group to the SM. They can potentially generate further contributions to ΔM_s , that depend on the specific breaking chain. A study of the UV completion for the V_2 vector leptoquark is, however, beyond the scope of this work, but will be required for a comprehensive analysis of loop-induced constraints on this vector state.

Remarkably, if we work in the basis of mass eigenstates $Q_i = (V_{ij} u_L^j, d_L^i)$ where the CKM mixing originates from the up sector, then a contribution to $\mathcal{B}(B_u \rightarrow \tau\nu)$ severely constrains the model. Nevertheless, this contribution can be easily suppressed by introducing $\beta_{1\tau}^{Qe}$ and enforcing some mild cancellation with $\beta_{2\tau}^{Qe}$ [48]. After integrating out V_2 and matching to the SMEFT, we obtain the following operator at tree-level

$$\mathcal{L}_{\text{SMEFT}}^{V_2} = \frac{[C_{ledq}]^{\tau\tau 32}}{M_{V_2}^2} [Q_{ledq}^\dagger]^{\tau\tau 23} = \frac{2\beta_{3\tau}^{dL} (\beta_{2\tau}^{Qe})^*}{M_{V_2}^2} \times [Q_{ledq}^\dagger]^{\tau\tau 23}, \tag{4.6}$$

which at low energies matches into,

$$[C_{vedu}^{S,RL}]^{332*}(m_b) = -\eta_S^{\tau\nu} [C_{ledq}]^{\tau\tau 32} (M_{V_2}) \frac{v^2}{2V_{cb} M_{V_2}^2}, \tag{4.7}$$

$$[C_{ed}^{S,LR}]^{323}(m_b) = -\eta_S^{\tau\tau} [C_{ledq}]^{\tau\tau 32} (M_{V_2}) \frac{v^2}{2M_{V_2}^2}. \tag{4.8}$$

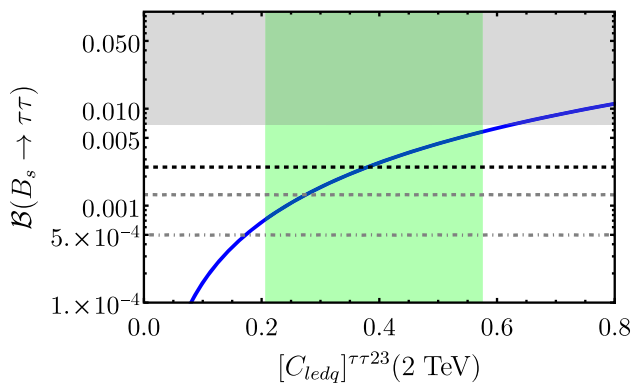


Fig. 4 V_2 model prediction for $\mathcal{B}(B_s \rightarrow \tau\tau)$ (blue line) as a function of the SMEFT Wilson coefficient $[C_{ledq}]^{\tau\tau 23}$. The current 95% CL excluded region by LHCb is grey shaded. The dashed black line depicts the projected 95% CL indirect bound obtained from τ_{B_s}/τ_{B_d} . The gray dashed and dashed-dotted lines represent the projected 95% CL direct bounds by LHCb for 50 fb^{-1} and 300 fb^{-1} , respectively

Notice that this is the same operator predicted by the U_1 leptoquark in models featuring third family quark-lepton unification, as discussed in the previous section. As such, it provides chiral enhancement of $\mathcal{B}(B_s \rightarrow \tau\tau)$ via $C_S^{\tau\tau} = -C_P^{\tau\tau}$, obtained from $\left[C_{ed}^{S,LR}\right]^{3323}$ when applying Eq. (C.9).

The scalar operator $\left[C_{vedu}^{S,RL}\right]^{3332*}$ provides a large contribution to R_D , able to fit the current experimental central value, while the contribution to R_{D^*} accommodates only marginally the current tension (see Eqs. (C.2) and (C.3)). In Fig. 4, we show the model prediction for $\mathcal{B}(B_s \rightarrow \tau\tau)$ as a function of $[C_{ledq}]^{\tau\tau 23}$ (2 TeV). We can see that the current direct bound by LHCb is unable to constrain the region preferred at 1σ by R_D . Nevertheless, in the near future we expect the indirect bound from the lifetime ratio τ_{B_s}/τ_{B_d} to provide a leading constraint over the model. Being more specific, τ_{B_s}/τ_{B_d} will constrain the model from explaining the central values of R_D (or larger). In the much longer term, LHCb has the potential to fully test the model with 300 fb^{-1} of integrated luminosity.

5 Conclusions

Several new physics scenarios proposed to address anomalies in B -physics naturally predict an enhancement of $b \rightarrow s\tau\tau$. In this work, we have explored the impact of new physics in the $b \rightarrow s\tau\tau$ channel over the lifetime ratio τ_{B_s}/τ_{B_d} and the lifetime difference $\Delta\Gamma_s$. First of all, via a model-independent analysis, we assessed the constraining power of the lifetime ratio and lifetime difference over NP in $b \rightarrow s\tau\tau$. We conclude that such observables provide indirect bounds over new physics scenarios, which, however, are not currently competitive with the existing direct experimental bounds.

Nevertheless, we have estimated future projections and concluded that both τ_{B_s}/τ_{B_d} and $\Delta\Gamma_s$ can provide competitive bounds before the LHCb and Belle II experiments reach the large integrated luminosities required to improve their direct bounds on $b \rightarrow s\tau\tau$ transitions. By looking at the different NP operators, we find that the lifetime ratio can potentially constrain scenarios where $\mathcal{B}(B_s \rightarrow \tau\tau)$ is enhanced. On the other hand, the lifetime difference is very interesting in scenarios where $\mathcal{B}(B_s \rightarrow \tau\tau)$ is not modified by NP couplings, and also to constrain scenarios with similar NP couplings for left-handed and right-handed quarks. We also introduce simplified models that can address $R_{D^{(*)}}$ without generating tree-level contributions to the neutral meson mass differences. Two scenarios are particularly interesting, namely the ones of the vector leptoquarks $U_1 \sim (\mathbf{3}, \mathbf{1}, 2/3)$ and $V_2 \sim (\bar{\mathbf{3}}, \mathbf{2}, 5/6)$. In fact, in these scenarios τ_{B_s}/τ_{B_d} can provide competitive constraints in the near future, thanks to a chiral enhancement of $\mathcal{B}(B_s \rightarrow \tau\tau)$ provided by scalar low-energy operators. This work motivates efforts by both the theoretical and experimental communities to investigate τ_{B_s}/τ_{B_d} and $\Delta\Gamma_s$ as potential channels to constrain NP effects.

Acknowledgements We thank Claudia Cornella and Gino Isidori for useful comments on this manuscript. We thank Miguel Escudero for pointing out a typo in Appendix C. The work of MFN is supported by the European Union's Horizon 2020 Research and Innovation Programme under Marie Skłodowska-Curie grant agreement HIDDEN European ITN project (H2020-MSCA-ITN-2019//860881-HIDDEN). MFN is grateful to the CERN Theory Division for the hospitality during parts of this work.

Data availability statement This manuscript has no associated data or the data will not be deposited. [Authors' comment: The external experimental data used in this analysis is publicly available through the references listed in the bibliography.]

Open Access This article is licensed under a Creative Commons Attribution 4.0 International License, which permits use, sharing, adaptation, distribution and reproduction in any medium or format, as long as you give appropriate credit to the original author(s) and the source, provide a link to the Creative Commons licence, and indicate if changes were made. The images or other third party material in this article are included in the article's Creative Commons licence, unless indicated otherwise in a credit line to the material. If material is not included in the article's Creative Commons licence and your intended use is not permitted by statutory regulation or exceeds the permitted use, you will need to obtain permission directly from the copyright holder. To view a copy of this licence, visit <http://creativecommons.org/licenses/by/4.0/>.

Funded by SCOAP³. SCOAP³ supports the goals of the International Year of Basic Sciences for Sustainable Development.

A Operator basis

In this Appendix, we list all the operators that we use in our analysis. In the SMEFT [7] we have:

$$\begin{aligned}
 [Q_{lq}^{(1)}]^{\alpha\beta ij} &= (\bar{L}^\alpha \gamma^\mu L^\beta)(\bar{Q}^i \gamma^\mu Q^j) \\
 [Q_{lq}^{(3)}]^{\alpha\beta ij} &= (\bar{L}^\alpha \gamma^\mu \sigma^a L^\beta)(\bar{Q}^i \gamma^\mu \sigma^a Q^j)
 \end{aligned}
 \tag{A.1}$$

$$\begin{aligned}
 [Q_{ed}]^{\alpha\beta ij} &= (\bar{e}_R^\alpha \gamma_\mu e_R^\beta)(\bar{d}_R^i \gamma^\mu d_R^j) \\
 [Q_{ld}]^{\alpha\beta ij} &= (\bar{L}^\alpha \gamma^\mu L^\beta)(\bar{d}_R^i \gamma^\mu d_R^j)
 \end{aligned}
 \tag{A.2}$$

$$\begin{aligned}
 [Q_{ledq}]^{\alpha\beta ij} &= (\bar{L}_a^\alpha e_R^\beta)(\bar{d}_R^i Q_a^j) \\
 [Q_{qe}]^{\alpha\beta ij} &= (\bar{Q}^\alpha \gamma^\mu Q^\beta)(\bar{e}_R^i \gamma^\mu e_R^j).
 \end{aligned}
 \tag{A.3}$$

and we work in the basis: $Q^{i,T} = (V_{ij}^* u_L^j, d_L^i)$ and $L^{i,T} = (U_{ij}^* \nu_j, e_L^i)$, where V and U denote the CKM and PMNS matrices, respectively.

In the LEFT [8,49], we use the following FCNCs operators:

$$\begin{aligned}
 [O_{ed}^{V,LL}]^{\alpha\beta ij} &= (\bar{\ell}^\alpha \gamma_\mu P_L \ell^\beta)(\bar{d}^i \gamma^\mu P_L d^j) \\
 [O_{ed}^{V,RR}]^{\alpha\beta ij} &= (\bar{\ell}^\alpha \gamma_\mu P_R \ell^\beta)(\bar{d}^i \gamma^\mu P_R d^j)
 \end{aligned}
 \tag{A.4}$$

$$\begin{aligned}
 [O_{ed}^{V,LR}]^{\alpha\beta ij} &= (\bar{\ell}^\alpha \gamma_\mu P_L \ell^\beta)(\bar{d}^i \gamma^\mu P_R d^j) \\
 [O_{ed}^{V,RL}]^{\alpha\beta ij} &= (\bar{\ell}^\alpha \gamma_\mu P_R \ell^\beta)(\bar{d}^i \gamma^\mu P_L d^j)
 \end{aligned}
 \tag{A.5}$$

$$\begin{aligned}
 [O_{ed}^{S,RR}]^{\alpha\beta ij} &= (\bar{\ell}^\alpha P_R \ell^\beta)(\bar{d}^i P_R d^j) \\
 [O_{ed}^{S,RL}]^{\alpha\beta ij} &= (\bar{\ell}^\alpha P_R \ell^\beta)(\bar{d}^i P_L d^j)
 \end{aligned}
 \tag{A.6}$$

$$\begin{aligned}
 [O_{ed}^{S,LL}]^{\alpha\beta ij} &= (\bar{\ell}^\alpha P_L \ell^\beta)(\bar{d}^i P_L d^j) \\
 [O_{ed}^{S,LR}]^{\alpha\beta ij} &= (\bar{\ell}^\alpha P_L \ell^\beta)(\bar{d}^i P_R d^j)
 \end{aligned}
 \tag{A.7}$$

$$\begin{aligned}
 [O_{ed}^{T,RR}]^{\alpha\beta ij} &= (\bar{\ell}^\alpha \sigma_{\mu\nu} P_R \ell^\beta)(\bar{d}^i \sigma^{\mu\nu} P_R d^j) \\
 [O_{ed}^{T,LL}]^{\alpha\beta ij} &= (\bar{\ell}^\alpha \sigma_{\mu\nu} P_L \ell^\beta)(\bar{d}^i \sigma^{\mu\nu} P_L d^j),
 \end{aligned}
 \tag{A.8}$$

the charged current operators:

$$\begin{aligned}
 [O_{vedu}^{V,LL}]^{\alpha\beta ij} &= (\bar{\nu}^\alpha \gamma^\mu P_L \ell^\beta)(\bar{d}^i \gamma_\mu P_L u^j) \\
 [O_{vedu}^{V,LR}]^{\alpha\beta ij} &= (\bar{\nu}^\alpha \gamma^\mu P_L \ell^\beta)(\bar{d}^i \gamma_\mu P_R u^j)
 \end{aligned}
 \tag{A.9}$$

$$\begin{aligned}
 [O_{vedu}^{S,RR}]^{\alpha\beta ij} &= (\bar{\nu}^\alpha P_R \ell^\beta)(\bar{d}^i P_R u^j) \\
 [O_{vedu}^{S,RL}]^{\alpha\beta ij} &= (\bar{\nu}^\alpha P_R \ell^\beta)(\bar{d}^i P_L u^j)
 \end{aligned}
 \tag{A.10}$$

$$[O_{vedu}^{T,RR}]^{\alpha\beta ij} = (\bar{\nu}^\alpha \sigma^{\mu\nu} P_R \ell^\beta)(\bar{d}^i \sigma^{\mu\nu} P_R u^j)
 \tag{A.11}$$

and the four-quark operators:

$$\begin{aligned}
 [O_{dd}^{V,LL}]^{ijkl} &= (\bar{d}_L^i \gamma_\mu d_L^j)(\bar{d}_L^k \gamma^\mu d_L^l) \\
 [O_{dd}^{V,RR}]^{ijkl} &= (\bar{d}_R^i \gamma_\mu d_R^j)(\bar{d}_R^k \gamma^\mu d_R^l)
 \end{aligned}
 \tag{A.12}$$

$$\begin{aligned}
 [O_{dd}^{V1,LR}]^{ijkl} &= (\bar{d}_L^i \gamma_\mu d_L^j)(\bar{d}_R^k \gamma^\mu d_R^l) \\
 [O_{dd}^{V8,RR}]^{ijkl} &= (\bar{d}_L^i \gamma_\mu T^a d_L^j)(\bar{d}_R^k \gamma^\mu T^a d_R^l)
 \end{aligned}
 \tag{A.13}$$

$$\begin{aligned}
 [O_{dd}^{S1,RR}]^{ijkl} &= (\bar{d}_L^i d_R^j)(\bar{d}_L^k d_R^l) \\
 [O_{dd}^{S8,RR}]^{ijkl} &= (\bar{d}_L^i T^a d_R^j)(\bar{d}_L^k T^a d_R^l)
 \end{aligned}
 \tag{A.14}$$

Following the normalization of Eqs. (2.1) and (2.2), the tree-level matching for the operators relevant for $b \rightarrow s\tau\tau$ reads [49]

$$\begin{aligned}
 [C_{ed}^{V,LL}]^{3323} &= \frac{[\tilde{C}_{\ell q}^{(1)}]^{3323} v^2}{2\Lambda^2} + \frac{[\tilde{C}_{\ell q}^{(3)}]^{3323} v^2}{2\Lambda^2}, \\
 [C_{ed}^{V,RR}]^{3323} &= \frac{[\tilde{C}_{ed}]^{3323} v^2}{2\Lambda^2},
 \end{aligned}
 \tag{A.15}$$

$$\begin{aligned}
 [C_{ed}^{V,LR}]^{3323} &= \frac{[\tilde{C}_{\ell d}]^{3323} v^2}{2\Lambda^2}, \\
 [C_{de}^{V,LR}]^{3323} &= \frac{[\tilde{C}_{qe}]^{3323} v^2}{2\Lambda^2},
 \end{aligned}
 \tag{A.16}$$

$$\begin{aligned}
 [C_{ed}^{S,RR}]^{3323} &= 0, \\
 [C_{ed}^{S,RL}]^{3323} &= \frac{[\tilde{C}_{ledq}]^{3323} v^2}{2\Lambda^2},
 \end{aligned}
 \tag{A.17}$$

$$\begin{aligned}
 [C_{ed}^{S,LL}]^{3323} &= 0, \\
 [C_{ed}^{S,LR}]^{3323} &= \frac{[(\tilde{C}_{ledq})^*]^{3332} v^2}{2\Lambda^2},
 \end{aligned}
 \tag{A.18}$$

$$[C_{ed}^{T,RR}]^{3323} = 0, \quad [O_{ed}^{T,LL}]^{3323} = 0.
 \tag{A.19}$$

For the operators relevant for $b \rightarrow c\tau\bar{\nu}$, following the normalization of Eqs. (2.1) and (C.1) we have

$$\begin{aligned}
 [C_{vedu}^{V,LL}]^{3332} &= \frac{2[\tilde{C}_{\ell q}^{(3)}]^{3332} v^2}{2V_{cb}\Lambda^2}, \\
 [C_{vedu}^{V,LR}]^{3332} &= 0,
 \end{aligned}
 \tag{A.20}$$

$$\begin{aligned}
 [C_{vedu}^{S,RR}]^{\alpha\beta ij} &= \frac{[\tilde{C}_{\ell qu}^{(3)}]^{3332} v^2}{2V_{cb}\Lambda^2}, \\
 [C_{vedu}^{S,RL}]^{3332} &= \frac{[\tilde{C}_{ledq}]^{3332} v^2}{2V_{cb}\Lambda^2},
 \end{aligned}
 \tag{A.21}$$

$$[C_{vedu}^{T,RR}]^{3332} = \frac{[\tilde{C}_{lequ}^{(3)}]^{3332} v^2}{2V_{cb}\Lambda^2}. \tag{A.22}$$

where in all cases above we are assuming that NP do not modify the Z boson nor W boson couplings to fermions.

B Lattice input

The BSM bag parameters are taken from the averages in [50] and displayed in Table 2. They refer to the operators:

$$\mathcal{O}_1^s = (\bar{b}\gamma_\mu P_L s) (\bar{b}\gamma^\mu P_L s), \tag{B.1}$$

$$\mathcal{O}_2^s = (\bar{b} P_L s) (\bar{b} P_L s), \quad \mathcal{O}_3^s = (\bar{b}_\alpha P_L s_\beta) (\bar{b}_\beta P_L s_\alpha), \tag{B.2}$$

$$\mathcal{O}_4^s = (\bar{b} P_L s) (\bar{b} P_R s), \quad \mathcal{O}_5^s = (\bar{b}_\alpha P_L s_\beta) (\bar{b}_\beta P_R s_\alpha). \tag{B.3}$$

Their expectation values are given by:

$$\langle \mathcal{O}_1^s \rangle = c_1 f_{B_q}^2 M_{B_s}^2 B_{B_s}^{(1)}(\mu) \tag{B.4}$$

$$\langle \mathcal{O}_i^s \rangle = c_i \left(\frac{M_{B_s}}{m_b(\mu) + m_s(\mu)} \right)^2 f_{B_q}^2 M_{B_s}^2 B_{B_s}^{(i)}(\mu), \quad i = 2, 3 \tag{B.5}$$

$$\langle \mathcal{O}_i^s \rangle = c_i \left(\frac{M_{B_s}}{m_b(\mu) + m_s(\mu)} + d_i \right)^2 f_{B_q}^2 M_{B_s}^2 B_{B_s}^{(i)}(\mu), \quad i = 4, 5 \tag{B.6}$$

where $c_i = \{2/3, -5/12, 1/12, 1/2, 1/6\}$, $d_4 = 1/6$ and $d_5 = 3/2$. The same bag parameters apply for the set of $P_L \longleftrightarrow P_R$ operators. Remember $P_{L,R} = (1 \pm \gamma_5)/2$. We also use $f_{B_s} = 230.3 \pm 1.3$ MeV [51] and $M_{B_s} = 5366.92 \pm 0.10$ MeV [52] as input values.

C Semileptonic observables

C.1 $b \rightarrow c\tau\nu$

We are interested in the following operators from the effective Lagrangian describing $b \rightarrow c\tau\bar{\nu}$ transition,

$$\mathcal{L}_{b \rightarrow c\tau\nu} = -\frac{4G_F}{\sqrt{2}} V_{cb} \left[\left(1 + [C_{vedu}^{V,LL}]^{3332*} \right) [\mathcal{O}_{vedu}^{V,LL}]^{3332\dagger} + [C_{vedu}^{S,RL}]^{3332*} [\mathcal{O}_{vedu}^{S,RL}]^{3332\dagger} + \text{h.c.} \right] \tag{C.1}$$

where the Wilson coefficients are at the m_b scale. The observables driving the NP effects are the universality ratios $R_{D^{(*)}}$:

$$R_D = R_D^{\text{SM}} \left[1 + [C_{vedu}^{V,LL}]^{3332*} \right]^2$$

$$+ 1.5 \text{Re} \left\{ \left(1 + [C_{vedu}^{V,LL}]^{3332*} \right) [C_{vedu}^{S,RL}]^{3332*} \right\} + 1.03 \left[[C_{vedu}^{S,RL}]^{3332*} \right]^2, \tag{C.2}$$

$$R_{D^*} = R_{D^*}^{\text{SM}} \left[1 + [C_{vedu}^{V,LL}]^{3332*} \right]^2 + 0.12 \text{Re} \left\{ \left(1 + [C_{vedu}^{V,LL}]^{3332*} \right) [C_{vedu}^{S,RL}]^{3332*} \right\} + 0.04 \left[[C_{vedu}^{S,RL}]^{3332*} \right]^2, \tag{C.3}$$

where $R_D^{\text{SM}} = 0.298 \pm 0.004$ and $R_{D^*}^{\text{SM}} = 0.254 \pm 0.005$ [1], and the numerical coefficients are obtained from integrating over the full kinematical distributions for the $B \rightarrow D^{(*)}$ semileptonic decay [53,54].

C.2 $b \rightarrow s\tau\tau$

In order to express in a simpler way the observables in the $b \rightarrow s\tau\tau$ channel, it is convenient to adopt a different operator basis than the one in Eqs. (A.4)–(A.8). We introduce:

$$\mathcal{O}_9^{\tau\tau} = (\bar{s}\gamma_\mu P_L b) (\bar{\tau}\gamma^\mu \tau), \quad \mathcal{O}_S^{\tau\tau} = (\bar{s} P_R b) (\bar{\tau} \tau) \tag{C.4}$$

$$\mathcal{O}_{10}^{\tau\tau} = (\bar{s}\gamma_\mu P_L b) (\bar{\tau}\gamma^\mu \gamma_5 \tau), \quad \mathcal{O}_P^{\tau\tau} = (\bar{s} P_R b) (\bar{\tau} \gamma_5 \tau), \tag{C.5}$$

which give rise to the following effective Lagrangian:

$$\mathcal{L}_{b \rightarrow s\tau\tau} = \frac{4G_F}{\sqrt{2}} V_{ts}^* V_{tb} \frac{\alpha}{4\pi} \left[(C_9^{\text{SM}} + C_9^{\tau\tau}) \mathcal{O}_9^{\tau\tau} + (C_{10}^{\text{SM}} + C_{10}^{\tau\tau}) \mathcal{O}_{10}^{\tau\tau} + C_S^{\tau\tau} \mathcal{O}_S^{\tau\tau} + C_P^{\tau\tau} \mathcal{O}_P^{\tau\tau} + \text{h.c.} \right], \tag{C.6}$$

where for simplicity we suppressed the scale dependence of the Wilson coefficients, which are at the scale $\mu = m_b$. The SM values are given by $C_9^{\text{SM}} = 4.27$ and $C_{10}^{\text{SM}} = -4.17$ [55]. With these definitions, the expressions for the observables of interest read [31,56]

$$\mathcal{B}(B_s \rightarrow \tau\tau) = \mathcal{B}(B_s \rightarrow \tau\tau)^{\text{SM}} \left\{ \left| 1 + \frac{C_{10}^{\tau\tau}}{C_{10}^{\text{SM}}} + \frac{C_P^{\tau\tau}}{C_{10}^{\text{SM}}} \times \frac{M_{B_s}^2}{2m_\tau(m_b + m_s)} \right|^2 + \left(1 - \frac{4m_\tau^2}{M_{B_s}^2} \right) \left| \frac{C_S^{\tau\tau}}{C_{10}^{\text{SM}}} \frac{M_{B_s}^2}{2m_\tau(m_b + m_s)} \right|^2 \right\} \tag{C.7}$$

Table 2 Bag parameters $B_{B_s}^{(i)}$ in the $\overline{\text{MS}}$ scheme evaluated at the scale $\mu = \overline{m}_b$. The values displayed are the averages taken from [50]

i	1	2	3	4	5
$B_{B_s}^{(i)}$	0.84(3)	0.83(4)	0.85(5)	1.03(4)	0.94(3)

$$\begin{aligned}
 \mathcal{B}(B^+ \rightarrow K^+ \tau \tau) &= 10^{-9} \left(2.2 |C_9^{\tau\tau} + C_9^{\text{SM}}|^2 + 6.0 |C_{10}^{\tau\tau} + C_{10}^{\text{SM}}|^2 \right. \\
 &\quad + 8.3 |C_S^{\tau\tau}|^2 + 8.9 |C_P^{\tau\tau}|^2 \\
 &\quad + 4.8 \text{Re}[C_S^{\tau\tau}(C_9^{\tau\tau} + C_9^{\text{SM}})^*] \\
 &\quad \left. + 5.9 \text{Re}[C_P^{\tau\tau}(C_{10}^{\tau\tau} + C_{10}^{\text{SM}})^*] \right), \quad (\text{C.8})
 \end{aligned}$$

where we use $\mathcal{B}(B_s \rightarrow \tau \tau)_{\text{SM}} = (7.73 \pm 0.49) \cdot 10^{-7}$ [57] and $\mathcal{B}(B^+ \rightarrow K^+ \tau \tau)_{\text{SM}} = (1.4 \pm 0.2) \cdot 10^{-7}$ [58]. The numerical values for the NP contributions to $B^+ \rightarrow K^+ \tau \tau$ decays are taken from [31, 58].

The operators $C_9^{\tau\tau}$ and $C_{10}^{\tau\tau}$ are related to $[C_{ed}^{V,LL}]^{3323}$ and $[C_{de}^{V,LR}]^{3323}$ via

$$\begin{aligned}
 C_9^{\tau\tau} &= \frac{2\pi}{\alpha V_{ts}^* V_{tb}} \left([C_{ed}^{V,LL}]^{3323} + [C_{de}^{V,LR}]^{3323} \right), \\
 C_{10}^{\tau\tau} &= \frac{2\pi}{\alpha V_{ts}^* V_{tb}} \left([C_{de}^{V,LR}]^{3323} - [C_{ed}^{V,LL}]^{3323} \right). \quad (\text{C.9})
 \end{aligned}$$

The operators $[C_{ed}^{S,LL}]^{3323}$ and $[C_{ed}^{S,LR}]^{3323}$ are related to $C_S^{\tau\tau}$ and $C_P^{\tau\tau}$ via

$$\begin{aligned}
 C_S^{\tau\tau} &= \frac{2\pi}{\alpha V_{ts}^* V_{tb}} \left([C_{ed}^{S,RR}]^{3323} - [C_{ed}^{S,LR}]^{3323} \right), \\
 C_P^{\tau\tau} &= \frac{2\pi}{\alpha V_{ts}^* V_{tb}} \left([C_{ed}^{S,RR}]^{3323} + [C_{ed}^{S,LR}]^{3323} \right). \quad (\text{C.10})
 \end{aligned}$$

References

1. HFLAV Collaboration, Y. Amhis et al., Averages of b -hadron, c -hadron, and τ -lepton properties as of 2021. [arXiv:2206.07501](https://arxiv.org/abs/2206.07501) [hep-ex]
2. Fermilab Lattice, MILC, Fermilab Lattice, MILC Collaboration, A. Bazavov et al., Semileptonic form factors for $B \rightarrow D^* \ell \nu$ at nonzero recoil from 2 + 1-flavor lattice QCD: Fermilab Lattice and MILC Collaborations. *Eur. Phys. J. C* **82**(12), 1141 (2022). <https://doi.org/10.1140/epjc/s10052-022-10984-9>. [arXiv:2105.14019](https://arxiv.org/abs/2105.14019) [hep-lat]. [Erratum: *Eur.Phys.J.C* 83, 21 (2023)]
3. J. Harrison, C. T. H. Davies, $B \rightarrow D^*$ vector, axial-vector and tensor form factors for the full q^2 range from lattice QCD. [arXiv:2304.03137](https://arxiv.org/abs/2304.03137) [hep-lat]
4. JLQCD Collaboration, Y. Aoki, B. Colquhoun, H. Fukaya, S. Hashimoto, T. Kaneko, R. Kellermann, J. Koponen, E. Kou, $B \rightarrow D^* \ell \nu_\ell$ semileptonic form factors from lattice QCD with Möbius domain-wall quarks. [arXiv:2306.05657](https://arxiv.org/abs/2306.05657) [hep-lat]
5. LHCb Collaboration, R. Aaij et al., Measurement of the ratio of branching fractions $\mathcal{B}(B_c^+ \rightarrow J/\psi \tau^+ \nu_\tau) / \mathcal{B}(B_c^+ \rightarrow J/\psi \mu^+ \nu_\mu)$. *Phys. Rev. Lett.* **120**(12), 121801 (2018). <https://doi.org/10.1103/PhysRevLett.120.121801>. [arXiv:1711.05623](https://arxiv.org/abs/1711.05623) [hep-ex]

6. LHCb Collaboration, R. Aaij et al., Observation of the decay $\Lambda_b^0 \rightarrow \Lambda_c^+ \tau^- \bar{\nu}_\tau$. *Phys. Rev. Lett.* **128**(19), 191803, (2022). <https://doi.org/10.1103/PhysRevLett.128.191803>. [arXiv:2201.03497](https://arxiv.org/abs/2201.03497) [hep-ex]
7. B. Grzadkowski, M. Iskrzynski, M. Misiak, J. Rosiek, Dimension-six terms in the standard model Lagrangian. *JHEP* **10**, 085 (2010). [https://doi.org/10.1007/JHEP10\(2010\)085](https://doi.org/10.1007/JHEP10(2010)085). [arXiv:1008.4884](https://arxiv.org/abs/1008.4884) [hep-ph]
8. E.E. Jenkins, A.V. Manohar, P. Stoffer, Low-energy effective field theory below the electroweak scale: anomalous dimensions. *JHEP* **01**, 084 (2018). [https://doi.org/10.1007/JHEP01\(2018\)084](https://doi.org/10.1007/JHEP01(2018)084). [arXiv:1711.05270](https://arxiv.org/abs/1711.05270) [hep-ph]
9. J. Fuentes-Martin, P. Ruiz-Femenia, A. Vicente, J. Virto, DsixTools 2.0: The Effective Field Theory Toolkit. *Eur. Phys. J. C* **81**(2), 167 (2021). <https://doi.org/10.1140/epjc/s10052-020-08778-y>. [arXiv:2010.16341](https://arxiv.org/abs/2010.16341) [hep-ph]
10. C. Bobeth, U. Haisch, New Physics in Γ_{12}^s : $(\bar{s}b)(\bar{\tau}\tau)$ Operators. *Acta Phys. Polon. B* **44**, 127–176 (2013). <https://doi.org/10.5506/APhysPolB.44.127>. [arXiv:1109.1826](https://arxiv.org/abs/1109.1826) [hep-ph]
11. C. Bobeth, U. Haisch, A. Lenz, B. Pecjak, G. Tetlalmatzi-Xolocotzi, On new physics in $\Delta\Gamma_d$. *JHEP* **06**, 040 (2014). [https://doi.org/10.1007/JHEP06\(2014\)040](https://doi.org/10.1007/JHEP06(2014)040). [arXiv:1404.2531](https://arxiv.org/abs/1404.2531) [hep-ph]
12. M. Gerlach, U. Nierste, V. Shtabovenko, M. Steinhauser, Width Difference in the B-B⁻ System at Next-to-Next-to-Leading Order of QCD. *Phys. Rev. Lett.* **129**(10), 102001 (2022). <https://doi.org/10.1103/PhysRevLett.129.102001>. [arXiv:2205.07907](https://arxiv.org/abs/2205.07907) [hep-ph]
13. A. Lenz, Ultimate theory precision of meson mixing observables. FCC Flavour Physics Programme Workshop, 9, (2022). https://indico.cern.ch/event/1186057/contributions/5014305/attachments/2510453/4314750/Flavour@FCCee_2022.pdf
14. LHCb Collaboration, R. Aaij et al., Physics case for an LHCb Upgrade II - Opportunities in flavour physics, and beyond, in the HL-LHC era. [arXiv:1808.08865](https://arxiv.org/abs/1808.08865) [hep-ex]
15. A. Lenz, M.L. Piscopo, A.V. Rusov, Disintegration of beauty: a precision study. *JHEP* **01**, 004 (2023). [https://doi.org/10.1007/JHEP01\(2023\)004](https://doi.org/10.1007/JHEP01(2023)004). [arXiv:2208.02643](https://arxiv.org/abs/2208.02643) [hep-ph]
16. M. Bordone, B. Capdevila, P. Gambino, Three loop calculations and inclusive Vcb. *Phys. Lett. B* **822**, 136679 (2021). <https://doi.org/10.1016/j.physletb.2021.136679>. [arXiv:2107.00604](https://arxiv.org/abs/2107.00604) [hep-ph]
17. M. Bordone, P. Gambino, The semileptonic B_s and Λ_b widths. *PoS CKM2021*, 055 (2023). <https://doi.org/10.22323/1.411.0055>. [arXiv:2203.13107](https://arxiv.org/abs/2203.13107) [hep-ph]
18. P. Gambino, A. Melis, S. Simula, Extraction of heavy-quark-expansion parameters from unquenched lattice data on pseudoscalar and vector heavy-light meson masses. *Phys. Rev. D* **96**(1), 014511 (2017). <https://doi.org/10.1103/PhysRevD.96.014511>. [arXiv:1704.06105](https://arxiv.org/abs/1704.06105) [hep-lat]
19. P. Gambino, A. Melis, S. Simula, HQE parameters from unquenched lattice data on pseudoscalar and vector heavy-light meson masses. *EPJ Web Conf.* **175**, 13028 (2018). <https://doi.org/10.1051/epjconf/201817513028>. [arXiv:1710.10168](https://arxiv.org/abs/1710.10168) [hep-lat]
20. F. Bernlochner, M. Fael, K. Olschewsky, E. Persson, R. van Tonder, K.K. Vos, M. Welsch, First extraction of inclusive V_{cb} from q^2 moments. *JHEP* **10**, 068 (2022). [https://doi.org/10.1007/JHEP10\(2022\)068](https://doi.org/10.1007/JHEP10(2022)068). [arXiv:2205.10274](https://arxiv.org/abs/2205.10274) [hep-ph]
21. LHCb Collaboration, R. Aaij et al., Search for the decays $B_s^0 \rightarrow \tau^+ \tau^-$ and $B^0 \rightarrow \tau^+ \tau^-$. *Phys. Rev. Lett.* **118**(25), 251802 (2017). <https://doi.org/10.1103/PhysRevLett.118.251802>. [arXiv:1703.02508](https://arxiv.org/abs/1703.02508) [hep-ex]

22. Belle-II Collaboration, W. Altmannshofer, et al., The Belle II Physics Book. PTEP **2019**(12), 123C01 (2019). <https://doi.org/10.1093/ptep/ptz106>. arXiv:1808.10567 [hep-ex]. [Erratum: PTEP 2020, 029201 (2020)]
23. B. Capdevila, A. Crivellin, S. Descotes-Genon, L. Hofer, J. Matias, Searching for New Physics with $b \rightarrow s\tau^+\tau^-$ processes. Phys. Rev. Lett. **120**(18), 181802 (2018). <https://doi.org/10.1103/PhysRevLett.120.181802>. arXiv:1712.01919 [hep-ph]
24. I. Doršner, S. Fajfer, A. Greljo, J.F. Kamenik, N. Košnik, Physics of leptoquarks in precision experiments and at particle colliders. Phys. Rept. **641**, 1–68 (2016). <https://doi.org/10.1016/j.physrep.2016.06.001>. arXiv:1603.04993 [hep-ph]
25. A. Angelescu, D. Bečirević, D.A. Faroughy, F. Jaffredo, O. Sumensari, Single leptoquark solutions to the B-physics anomalies. Phys. Rev. D **104**(5), 055017 (2021). <https://doi.org/10.1103/PhysRevD.104.055017>. arXiv:2103.12504 [hep-ph]
26. M. Algueró, A. Biswas, B. Capdevila, S. Descotes-Genon, J. Matias, M. Novoa-Brunet, To (b)e or not to (b)e: No electrons at LHCb. arXiv:2304.07330 [hep-ph]
27. N.R. Singh Chundawat, New physics in $B \rightarrow K^*\tau^+\tau^-$: A model independent analysis. Phys. Rev. D **107**(5), 055004 (2023). <https://doi.org/10.1103/PhysRevD.107.055004>. arXiv:2212.01229 [hep-ph]
28. A. Crivellin, C. Greub, D. Müller, F. Saturnino, Importance of Loop Effects in Explaining the Accumulated Evidence for New Physics in B Decays with a Vector Leptoquark. Phys. Rev. Lett. **122**(1), 011805 (2019). <https://doi.org/10.1103/PhysRevLett.122.011805>. arXiv:1807.02068 [hep-ph]
29. A. Crivellin, B. Fuks, L. Schnell, Explaining the hints for lepton flavour universality violation with three S_2 leptoquark generations. JHEP **06**, 169 (2022). [https://doi.org/10.1007/JHEP06\(2022\)169](https://doi.org/10.1007/JHEP06(2022)169). arXiv:2203.10111 [hep-ph]
30. C. Cornella, J. Fuentes-Martin, G. Isidori, Revisiting the vector leptoquark explanation of the B-physics anomalies. JHEP **07**, 168 (2019). [https://doi.org/10.1007/JHEP07\(2019\)168](https://doi.org/10.1007/JHEP07(2019)168). arXiv:1903.11517 [hep-ph]
31. C. Cornella, D.A. Faroughy, J. Fuentes-Martin, G. Isidori, M. Neubert, Reading the footprints of the B-meson flavor anomalies. JHEP **08**, 050 (2021). [https://doi.org/10.1007/JHEP08\(2021\)050](https://doi.org/10.1007/JHEP08(2021)050). arXiv:2103.16558 [hep-ph]
32. A. Greljo, B.A. Stefanek, Third family quark-lepton unification at the TeV scale. Phys. Lett. B **782**, 131–138 (2018). <https://doi.org/10.1016/j.physletb.2018.05.033>. arXiv:1802.04274 [hep-ph]
33. L. Calibbi, A. Crivellin, T. Li, Model of vector leptoquarks in view of the B-physics anomalies. Phys. Rev. D **98**(11), 115002 (2018). <https://doi.org/10.1103/PhysRevD.98.115002>. arXiv:1709.00692 [hep-ph]
34. M. Blanke, A. Crivellin, B Meson Anomalies in a Pati-Salam Model within the Randall-Sundrum Background. Phys. Rev. Lett. **121**(1), 011801 (2018). <https://doi.org/10.1103/PhysRevLett.121.011801>. arXiv:1801.07256 [hep-ph]
35. L. Di Luzio, A. Greljo, M. Nardecchia, Gauge leptoquark as the origin of B-physics anomalies. Phys. Rev. D **96**(11), 115011 (2017). <https://doi.org/10.1103/PhysRevD.96.115011>. arXiv:1708.08450 [hep-ph]
36. L. Di Luzio, J. Fuentes-Martin, A. Greljo, M. Nardecchia, S. Renner, Maximal Flavour Violation: a Cabibbo mechanism for leptoquarks. JHEP **11**, 081 (2018). [https://doi.org/10.1007/JHEP11\(2018\)081](https://doi.org/10.1007/JHEP11(2018)081). arXiv:1808.00942 [hep-ph]
37. J. Aebischer, G. Isidori, M. Pesut, B.A. Stefanek, F. Wilsch, Confronting the vector leptoquark hypothesis with new low- and high-energy data. Eur. Phys. J. C **83**(2), 153 (2023). <https://doi.org/10.1140/epjc/s10052-023-11304-5>. arXiv:2210.13422 [hep-ph]
38. J.C. Pati, A. Salam, Lepton Number as the Fourth Color. Phys. Rev. D **10**, 275–289 (1974). <https://doi.org/10.1103/PhysRevD.10.275>. [Erratum: Phys.Rev.D 11, 703–703 (1975)]
39. M. Bordone, C. Cornella, J. Fuentes-Martin, G. Isidori, A three-site gauge model for flavor hierarchies and flavor anomalies. Phys. Lett. B **779**, 317–323 (2018). <https://doi.org/10.1016/j.physletb.2018.02.011>. arXiv:1712.01368 [hep-ph]
40. M. Bordone, C. Cornella, J. Fuentes-Martin, G. Isidori, Low-energy signatures of the PS^3 model: from B-physics anomalies to LFV. JHEP **10**, 148 (2018). [https://doi.org/10.1007/JHEP10\(2018\)148](https://doi.org/10.1007/JHEP10(2018)148). arXiv:1805.09328 [hep-ph]
41. L. Allwicher, G. Isidori, A.E. Thomsen, Stability of the Higgs Sector in a Flavor-Inspired Multi-Scale Model. JHEP **01**, 191 (2021). [https://doi.org/10.1007/JHEP01\(2021\)191](https://doi.org/10.1007/JHEP01(2021)191). arXiv:2011.01946 [hep-ph]
42. J. Fuentes-Martin, G. Isidori, J.M. Lizana, N. Selimovic, B.A. Stefanek, Flavor hierarchies, flavor anomalies, and Higgs mass from a warped extra dimension. Phys. Lett. B **834**, 137382 (2022). <https://doi.org/10.1016/j.physletb.2022.137382>. arXiv:2203.01952 [hep-ph]
43. J. Davighi, G. Isidori, M. Pesut, Electroweak-flavour and quark-lepton unification: a family non-universal path. JHEP **04**, 030 (2023). [https://doi.org/10.1007/JHEP04\(2023\)030](https://doi.org/10.1007/JHEP04(2023)030). arXiv:2212.06163 [hep-ph]
44. S.F. King, Twin Pati-Salam theory of flavour with a TeV scale vector leptoquark. JHEP **11**, 161 (2021). [https://doi.org/10.1007/JHEP11\(2021\)161](https://doi.org/10.1007/JHEP11(2021)161). arXiv:2106.03876 [hep-ph]
45. M. Fernández Navarro, S.F. King, B-anomalies in a twin Pati-Salam theory of flavour including the LHCb $R_{K^{(*)}}$ analysis. JHEP **02**(2023), 188 (2022). [https://doi.org/10.1007/JHEP02\(2023\)188](https://doi.org/10.1007/JHEP02(2023)188). arXiv:2209.00276 [hep-ph]
46. A. Celis, J. Fuentes-Martin, A. Vicente, J. Virto, DsixTools: The Standard Model Effective Field Theory Toolkit. Eur. Phys. J. C **77**(6), 405 (2017). <https://doi.org/10.1140/epjc/s10052-017-4967-6>. arXiv:1704.04504 [hep-ph]
47. J. Fuentes-Martin, G. Isidori, M. König, N. Selimović, Vector Leptoquarks Beyond Tree Level III: Vector-like Fermions and Flavor-Changing Transitions. Phys. Rev. D **102**, 115015 (2020). <https://doi.org/10.1103/PhysRevD.102.115015>. arXiv:2009.11296 [hep-ph]
48. S. Iguro, Y. Omura, A closer look at isodoublet vector leptoquark solution to $R_{D^{(*)}}$ anomaly. arXiv:2306.00052 [hep-ph]
49. E.E. Jenkins, A.V. Manohar, P. Stoffer, Low-Energy Effective Field Theory below the Electroweak Scale: Operators and Matching. JHEP **03**, 016 (2018). [https://doi.org/10.1007/JHEP03\(2018\)016](https://doi.org/10.1007/JHEP03(2018)016). arXiv:1709.04486 [hep-ph]
50. R.J. Dowdall, C.T.H. Davies, R.R. Horgan, G.P. Lepage, C.J. Monahan, J. Shigemitsu, M. Wingate, Neutral B-meson mixing from full lattice QCD at the physical point. Phys. Rev. D **100**(9), 094508 (2019). <https://doi.org/10.1103/PhysRevD.100.094508>. arXiv:1907.01025 [hep-lat]
51. Flavour Lattice Averaging Group (FLAG) Collaboration, Y. Aoki, et al., FLAG Review 2021. Eur. Phys. J. C **82**(10), 869 (2022). <https://doi.org/10.1140/epjc/s10052-022-10536-1>. arXiv:2111.09849 [hep-lat]
52. Particle Data Group Collaboration, R. L. Workman, et al., Review of Particle Physics. PTEP **2022** 083C01 (2022). <https://doi.org/10.1093/ptep/ptac097>
53. C. Murgui, A. Peñuelas, M. Jung, A. Pich, Global fit to $b \rightarrow c\tau\nu$ transitions. JHEP **09**, 103 (2019). [https://doi.org/10.1007/JHEP09\(2019\)103](https://doi.org/10.1007/JHEP09(2019)103). arXiv:1904.09311 [hep-ph]
54. R. Mandal, C. Murgui, A. Peñuelas, A. Pich, The role of right-handed neutrinos in $b \rightarrow c\tau\nu$ anomalies. JHEP **08**(08), 022 (2020). [https://doi.org/10.1007/JHEP08\(2020\)022](https://doi.org/10.1007/JHEP08(2020)022). arXiv:2004.06726 [hep-ph]
55. S. Bruggisser, R. Schäfer, D. van Dyk, S. Westhoff, The Flavor of UV Physics. JHEP **05**, 257 (2021). [https://doi.org/10.1007/JHEP05\(2021\)257](https://doi.org/10.1007/JHEP05(2021)257). arXiv:2101.07273 [hep-ph]

56. D. Bečirević, O. Sumensari, R. Zukanovich Funchal, Lepton flavor violation in exclusive $b \rightarrow s$ decays. Eur. Phys. J. C **76**(3), 134 (2016). <https://doi.org/10.1140/epjc/s10052-016-3985-0>. [arXiv:1602.00881](https://arxiv.org/abs/1602.00881) [hep-ph]
57. C. Bobeth, M. Gorbahn, T. Hermann, M. Misiak, E. Stamou, M. Steinhauser, $B_{s,d} \rightarrow l^+l^-$ in the Standard Model with Reduced Theoretical Uncertainty. Phys. Rev. Lett. **112**, 101801 (2014). <https://doi.org/10.1103/PhysRevLett.112.101801>. [arXiv:1311.0903](https://arxiv.org/abs/1311.0903) [hep-ph]
58. HPQCD Collaboration, C. Bouchard, G. P. Lepage, C. Monahan, H. Na, J. Shigemitsu, Standard Model Predictions for $B \rightarrow K \ell^+ \ell^-$ with Form Factors from Lattice QCD. Phys. Rev. Lett. **111**(16), 162002 (2013). <https://doi.org/10.1103/PhysRevLett.111.162002>. [arXiv:1306.0434](https://arxiv.org/abs/1306.0434) [hep-ph]. [Erratum: Phys.Rev.Lett. 112, 149902 (2014)]